Formation of the stress-induced ***mm***2 phase at the ferroelastic - antiferroelectric $\bar{4}3m$ - $\bar{4}2m$ phase transition in Cr - Cl boracite

1996 J. Phys.: Condens. Matter 8 6087

(http://iopscience.iop.org/0953-8984/8/33/015)

J. Phys.: Condens. Matter **8** (1996) 6087–6094. Printed in the UK

Formation of the stress-induced $mm2$ phase at the ferroelastic–antiferroelectric $\bar{4}3m$–$\bar{4}2m$ phase transition in Cr–Cl boracite

V Yu Topolov† and Z-G Ye‡

† Physics Faculty, Rostov State University, 344090 Rostov-on-Don, Russia

‡ Department of Inorganic, Analytical and Applied Chemistry, University of Geneva, CH-1211 Geneva 4, Switzerland

Received 5 January 1996, accepted for publication 20 May 1996

Abstract. Experimental and crystallographic investigations of the formation of the $mm2$ phase induced by internal stress at the $\bar{4}3m$–$\bar{4}2m$ phase boundaries during the first-order ferroelastic–antiferroelectric phase transition in $Cr_3B_7O_{13}Cl$ boracite crystals are presented. Different possibilities are demonstrated, by means of the determination of zero-net-strain planes, for the transformation from the tetragonal or the cubic phase to the orthorhombic one. The formation of the $mm2$ phase results in stress relief at the mechanically non-matching $\bar{4}3m$–$\bar{4}2m$ interfaces. Such a compromise role of the $mm2$ phase permits us to understand the mechanism of the stress-induced phase transition and the three-phase coexistence.

1. Introduction

Chromium–chlorine boracite $Cr_3B_7O_{13}Cl$ (Cr–Cl) has been found to undergo the following sequence of first-order structural phase transitions [1]:

$$\bar{4}3m \xleftrightarrow{T_1=264\ \mathrm{K}} \bar{4}2m \xleftrightarrow{T_2=160\ \mathrm{K}} mm2$$

where the tetragonal non-polar $\bar{4}2m$ phase (space group $P\bar{4}2_1c$ [2]) is the first and so far a unique one in the boracite family. In the temperature interval of the $\bar{4}2m$ phase ($T_1 < T < T_2$), application of an electric field $\boldsymbol{E} \parallel \langle 001\rangle_{cub} (> 8 \times 10^4$ V cm^{-1}) can induce a polar $mm2$ phase, giving rise to double hysteresis loops of 'antiferroelectric' behaviour [3, 4]. During the first-order transition from the cubic to the tetragonal phase at $T_1 = 264$ K, domains of the $mm2$ phase were found to be induced ephemerally by internal stress generated at the mechanically non-matching $\bar{4}3m$–$\bar{4}2m$ phase boundary [4]. The phase transition from $\bar{4}2m$ or $\bar{4}3m$ to $mm2$ can also be induced by applying a uniaxial stress ($> 10^7$ N m^{-2}) along $\langle 110\rangle_{cub}$ directions [5]. The magnetic ordering at low temperatures was revealed by anomalies of the spontaneous polarization and birefringence [6]. The onset of magnetic ordering and the symmetry of the magnetic phases were recently determined by studying the linear and quadratic magnetoelectric effects, i.e., antiferromagnetic $mm2$ for $T < 14$ K and weakly ferromagnetic $m'm'2$ for $T < 10$ K [7, 8].

The interest of the crystallographic investigation of the conditions for elastic matching of the phases with different symmetries and domain structures [9–12] is associated with the internal mechanical stress. This stress arises at the domain or phase boundaries and has an influence on the kinetics of phase transition, physical properties, etc, in the crystals. Some

0953-8984/96/336087+08$19.50

interesting features of the phase transition behaviour are also connected with coexistence of three phases, that occurs very seldom in ferroelectrics and related materials [13]. The present work is therefore devoted to the crystallographic analysis of the three-phase state related to the internal stress-induced phase transition at the ferroelastic–antiferroelectric $\bar{4}3m$–$\bar{4}2m$ phase transition in Cr–Cl boracite.

2. The stress-induced phase transition

The stress-induced phase transition has been disclosed by means of polarized light microscopy. Figure 1 shows photographs of domain states observed on the $(100)_{cub}$ and $(110)_{cub}$ platelets of Cr–Cl during the first-order $\bar{4}3m$–$\bar{4}2m$ phase transition at $T_1 = 264$ K. On the $(100)_{cub}$ plate, the induced $mm2$ phase can be identified by the domains with strong birefringence ($\Delta n = 6 \times 10^{-3}$ compared with $\Delta n = 3 \times 10^{-4}$ for the principal birefringence of the $\bar{4}2m$ phase) and the extinction directions parallel to $\langle 110 \rangle_{cub}$, which are characteristic of the ferroic species $\bar{4}3m1'Fmm21'$ [14]. On the $(110)_{cub}$ cut, the orthorhombic phase can be recognized by the domains of 'sea-gull' form with extinction direction oriented at about 45° to $\langle 110 \rangle_{cub}$. In both cases the induced $mm2$ phase was found to appear at the mechanically non-matching $\bar{4}3m$–$\bar{4}2m$ phase boundary and to propagate through the crystals during the phase transition. It disappeared when the crystal transformed completely from the cubic to the tetragonal phase or *vice versa*. Simultaneous measurement of the pseudo-pyroelectric charges indicated sharp pulses with opposite sign resulting from the appearance and disappearance of the induced domains, confirming the polar character of the induced $mm2$ phase.

Such an astonishing, ephemeral presence of the polar $mm2$ phase at the $\bar{4}3m$–$\bar{4}2m$ phase boundary, i.e., the three-phase coexistence of the $\bar{4}3m$, $\bar{4}2m$ and $mm2$ phases, can be understood thermodynamically on the basis of Gibbs' phase rule by admitting the presence of internal stress during the first-order $\bar{4}3m$–$\bar{4}2m$ phase transition, introducing an additional external constraint variable and hereby increasing the number of degrees of freedom by one.

3. Crystallographic analysis

The crystallographic examination of the phase coexistence in Cr–Cl was performed in terms of the basic paper by Metrat [9] and the other works [10], [11] and [15]. The simplest analysis shows that the $\bar{4}3m$ and $\bar{4}2m$ phases cannot be separated by a zero-net-strain plane because of violation of the necessary conditions [11]. The origin of the arising excess mechanical stress is associated with the simultaneous decrease of the unit cell parameters of the $\bar{4}2m$ phase ($a_t = b_t \neq c_t$) in comparison with that of the $\bar{4}3m$ phase (a_c): $a_t < a_c$ and $c_t < a_c$ [16]. Such a unit cell behaviour favours the coexistence of the single-domain $\bar{4}2m$ phase and the initial $\bar{4}3m$ one, as it may be derived from the minimization of the elastic interaction energy between these phases by using the method from [15]. In this case, in the vicinity of the temperature $T_1 = 264$ K, the $\bar{4}2m$ phase is separated from the $\bar{4}3m$ one in Cr–Cl by the deformed boundary connected with the significant anisotropy of the internal stress that finally favours the appearance of the induced $mm2$ phase, as well as the stress relief at the $\bar{4}3m$–$mm2$ and $\bar{4}2m$–$mm2$ interfaces. The analysis of the elastic matching gives different possibilities for determination of the zero-net-strain planes between the $\bar{4}2m$ and $mm2$ phases and between the $\bar{4}3m$ and $mm2$ ones, i.e. in the absence of the third phase.

From the symmetry point of view, both the cubic $\bar{4}3m$ and the tetragonal $\bar{4}2m$ phases can be transformed into the ferroelectric–ferroelastic $mm2$ one by stress components acting along

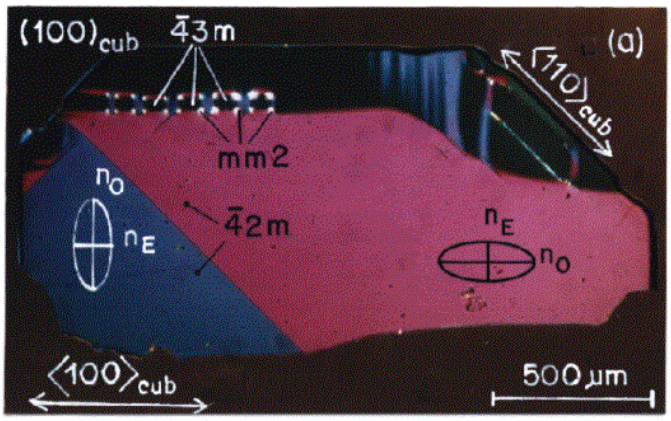

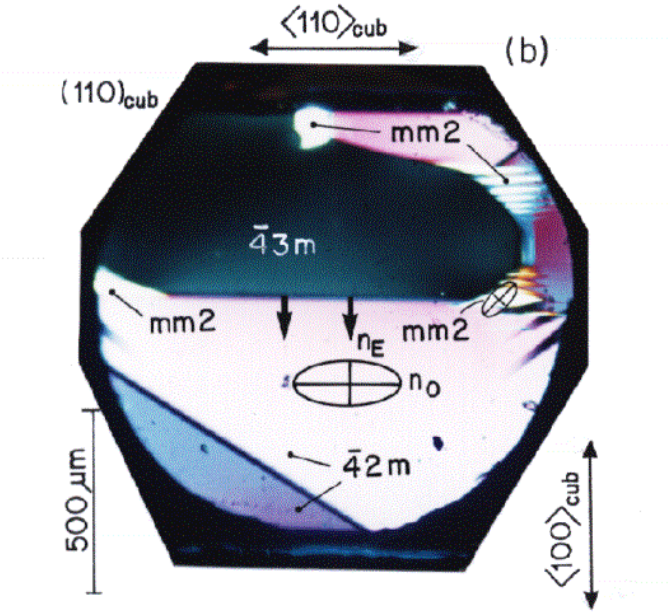

Figure 1. Optical domain structures revealing the internal stress-induced *mm*2 phase at the $\bar{4}3m$–$\bar{4}2m$ phase boundaries in Cr–Cl boracite during the $\bar{4}3m$–$\bar{4}2m$ phase transition (at $T_1 = 264$ K), leading to the coexistence of three phases, $\bar{4}3m$, $\bar{4}2m$ and *mm*2: (a) on a $(100)_{cub}$ platelet (thickness, 15 μm), during the $\bar{4}2m \rightarrow \bar{4}3m$ phase transition, with the induced *mm*2 phase appearing as a bright *rosette* form and (b) on a $(110)_{cub}$ platelet (thickness, 45 μm), during the $\bar{4}3m \rightarrow \bar{4}2m$ phase transition, with the induced *mm*2 phase appearing as bright *stripes* or a 'sea-gull' form (arrows indicate the direction of propagation of the phase boundary).

$\langle 110 \rangle_{cub}$ directions. As directly proved by experiments, application of a small uniaxial stress in the $\bar{4}2m$ phase along $\langle 110 \rangle_{cub}$ first results in the switching of the tetragonal ferroelastic domains with motion of the $(110)_{cub}$ walls. When the applied stress is higher than a threshold value of 12×10^7 N m^{-2}, the orthorhombic *mm*2 phase can actually be induced

from the $\bar{4}2m$ phase due to a symmetry breaking [5]. In the present case, however, the spontaneous stress is generated ephemerally due to the mechanical mismatching between the cubic phase and the tetragonal domains during the phase transition at 264 K. In the $\bar{4}2m$ phase, the mechanical energy is minimized by the formation of the tetragonal domain structure. The locally present spontaneous stress, created by the presence of the ferroelastic domains, is energetically equivalent for all the three tetragonal orientations and therefore has no effect on the ferroelastic domain switching. As we can see from the following quantitative analysis, the induction of the low-temperature orthorhombic $mm2$ phase allows the relief of the excess spontaneous stress and thereby the minimization of the free energy of the whole system. The induced $mm2$ phase is energetically close to the tetragonal phase since it appears spontaneously below 160 K without constraint. Such an induced $mm2$ phase remains pinned to the $\bar{4}3m$–$\bar{4}2m$ phase boundary during the first-order phase transition.

In order to describe the possibilities of the $\bar{4}2m$–$mm2$ elastic matching, it can be assumed that one of the three domains of the $\bar{4}2m$ phase (T_1, T_2 or T_3) may transform into domains of the $mm2$ phase, e.g. (1; 2), (3; 4) or (5; 6), as shown in figure 2. The corresponding distortion matrices may be written in the Cartesian coordinate system $(X_1X_2X_3)$ as

$$\|N^{(1)}\| = \begin{pmatrix} \eta_a & 0 & 0 \\ 0 & \eta_c & 0 \\ 0 & 0 & \eta_a \end{pmatrix} \qquad \|N^{(2)}\| = \begin{pmatrix} \eta_a & 0 & 0 \\ 0 & \eta_a & 0 \\ 0 & 0 & \eta_c \end{pmatrix} \qquad \|N^{(3)}\| = \begin{pmatrix} \eta_c & 0 & 0 \\ 0 & \eta_a & 0 \\ 0 & 0 & \eta_a \end{pmatrix}$$

for T_1, T_2 and T_3 domains of the $\bar{4}2m$ phase, respectively, as well as

$$\|P^{(1)}\| = p\begin{pmatrix} \epsilon_a & 0 & 0 \\ 0 & \epsilon_c & 0 \\ 0 & 0 & \epsilon_b \end{pmatrix} + (1-p)\begin{pmatrix} \cos\varphi_{ab} & 0 & -\sin\varphi_{ab} \\ 0 & 1 & 0 \\ \sin\varphi_{ab} & 0 & \cos\varphi_{ab} \end{pmatrix}\begin{pmatrix} \epsilon_b & 0 & 0 \\ 0 & \epsilon_c & 0 \\ 0 & 0 & \epsilon_a \end{pmatrix}$$

$$\|P^{(2)}\| = p\begin{pmatrix} \epsilon_a & 0 & 0 \\ 0 & \epsilon_b & 0 \\ 0 & 0 & \epsilon_c \end{pmatrix} + (1-p)\begin{pmatrix} \cos\varphi_{ab} & -\sin\varphi_{ab} & 0 \\ \sin\varphi_{ab} & \cos\varphi_{ab} & 0 \\ 0 & 0 & 1 \end{pmatrix}\begin{pmatrix} \epsilon_b & 0 & 0 \\ 0 & \epsilon_a & 0 \\ 0 & 0 & \epsilon_c \end{pmatrix}$$

$$\|P^{(3)}\| = p\begin{pmatrix} \epsilon_c & 0 & 0 \\ 0 & \epsilon_a & 0 \\ 0 & 0 & \epsilon_b \end{pmatrix} + (1-p)\begin{pmatrix} 1 & 0 & 0 \\ 0 & \cos\varphi_{ab} & -\sin\varphi_{ab} \\ 0 & \sin\varphi_{ab} & \cos\varphi_{ab} \end{pmatrix}\begin{pmatrix} \epsilon_c & 0 & 0 \\ 0 & \epsilon_b & 0 \\ 0 & 0 & \epsilon_a \end{pmatrix}$$

for the domain pairs (1; 2), (3; 4) and (5; 6) of the $mm2$ phase, respectively, where $\varphi_{ab} = \cos^{-1}[2\epsilon_a\epsilon_b/(\epsilon_a^2+\epsilon_b^2)]$ is the twinning angle; η_a and η_c are the unit cell distortions in the $\bar{4}2m$ phase and ϵ_a, ϵ_b and ϵ_c those in the $mm2$ phase, calculated by taking into account the rotation of the crystallographic axes with respect to the directions of the coordinate axes (OX_i) of the $\bar{4}3m$ phase and p and $(1-p)$ indicate the volume concentrations of different domain orientations $(1; 2; \ldots; 6)$.

The $\bar{4}2m$ and $mm2$ phases may match each other along the zero-net-strain planes by fulfilling the following conditions [9, 10, 15]:

$$\det\|D_{ij}\| = 0 \tag{1}$$

$$D_{ij}'^2 = D_{ij}^2 - D_{ii}D_{jj} \geqslant 0 \qquad (ij = 12; 13) \tag{2}$$

where the matrix elements $D_{ij} = \sum_{k=1}^{3}(N_{ik}^{(f)}N_{jk}^{(f)} - P_{ik}^{(g)}P_{jk}^{(g)})$ are determined by the corresponding elements of the distortion matrices $\|N^{(f)}\|$ and $\|P^{(g)}\|$ mentioned above; $f, g = 1; 2; 3$.

Results of the determination of the $\bar{4}2m$–$mm2$ phase boundaries as possible zero-net-strain planes are summarized in table 1. The orientations of these boundaries, calculated using the experimental data from [16] and the formulae from [9], [10] and [14] are approximated on the basis of the rational Miller indices $\{h\,k\,0\}_{cub}$ with an accuracy up

to 5%. One can establish some preferential transformations of single-domain $\bar{4}2m$ areas into polydomain $mm2$ phase, in accordance with the schemes $T_1 \rightarrow (1;2)$, $T_2 \rightarrow (3;4)$ or $T_3 \rightarrow (5;6)$, i.e. in the case of the parallel unit cell facets $(a_t; b_t)$ and $(a_0; b_0)$. The other variants of transformation $T_f \rightarrow (m; n)$ mentioned in table 1 do not allow the phase planes to match through the unstrained boundaries only. An important result is also obtained by using equations (1), (2) and the distortion matrices written above, if considering the possible domain types $(T_f; T_g)$ (instead of one such type) in the $\bar{4}2m$ phase as an initial structure for the further transformation into the $mm2$ phase, e.g. in the case of the domain structure reconstruction '$T_1 + T_2 \rightarrow (1;2)$'. The presence of the second ('excessive') domain type in the $\bar{4}2m$ phase does not favour the effective stress relief at phase boundaries, but can strongly influence the phase transition kinetics. An analogous effect was reported earlier in the description of the highly twinned ferro- and antiferroelectric perovskite-type crystals [17]. These crystals contain at least three domain types with a wide temperature range of stability for the orthorhombic phase, and their unit cell vectors $\boldsymbol{a}$, $\boldsymbol{b}$ and $\boldsymbol{c}$ satisfy the conditions of cyclic permutation.

There are also some unusual possibilities for the formation of the unstrained $\bar{4}2m$–$mm2$ phase boundaries, leading to appearance of the induced $mm2$ phase with different orientations of the faces $(a_0; b_0)$. Such domains may form independently in the adjacent crystal areas in the presence of stress. For example, in the transformation $T_2 \rightarrow (3;1)$ (see figure 2), the zero-net-strain planes are permitted for the optimal volume concentrations of the first domain type

$$p'_{opt} = (\pm\eta_c - \epsilon_c \cos\varphi_{bc})/(\epsilon_b - \epsilon_c \cos\varphi_{bc}). \tag{3}$$

Equation (3) is derived from (1) by using the corresponding distortion matrices of the $\bar{4}2m$ and $mm2$ phases and by neglecting the small values of $\sin^2\varphi_{bc} \rightarrow 0$, where $\varphi_{bc} = \cos^{-1}[2\epsilon_b\epsilon_c/(\epsilon_b^2 + \epsilon_c^2)]$. The related value of the optimal volume concentration from the interval $0 \leqslant p'_{opt} \leqslant 1$ is $p'_{\mathrm{opt}} = 0.549$, and the $\bar{4}2m$–$mm2$ phase boundary is described by the Miller indices $(3\,4\,0)_{cub}$ and/or $(\bar{3}\,4\,0)_{cub}$ in the $(X_1X_2X_3)$ system.

Different variants of the unstrained $\bar{4}2m$–$mm2$ phase boundaries are possible by the formation of the polydomain $mm2$ phase (table 1). Hence the appearance of the $mm2$ phase in the stress field may be associated with the realization of some conditions for stress relief, including a violation of the elastic matching at phase boundaries or, as a compromise, wedging the small regions of the $mm2$ phase [1, 3]. The last circumstance may be associated, for example, with differences between the polydomain areas of the $mm2$ phase appearing independently in different parts of the crystal (domain pairs (m, n) and optimal concentrations p_{opt} from table 1 or p'_{opt} from (3)). It should be noted that the separated parts of the $\{h\,k\,0\}_{cub}$ phase boundaries determined in the present work are in good agreement with the boundaries surrounding the 'sea-gull' shape domains of the $mm2$ phase (figure 1). This experimental fact testifies to our opinion on the compromise role of the mechanical-stress-induced $mm2$ phase which may be responsible for further effective stress relief in Cr–Cl crystals.

It becomes clear after our analysis based on the results of [11] and [15] that the presence of the above-mentioned 'excessive' domain type in the initial $\bar{4}2m$ phase can lead to the appearance of considerable stress fields ($\sim$ 10–100 MPa†) in the phase transition region and to the search for more complicated ways of relieving stress, especially in the presence of wedge- or zigzag-like domain boundaries. Some previous estimations show that a direct use of the formulae given by Metrat [9] is insufficient because of the necessity to take into

† These values are obtained by using the experimental data on the crystal structure of Cr–Cl [16] and the elastic properties of the related boracites [18].

Table 1. Elastic matching and zero-net-strain planes along $\bar{4}2m$–$mm2$ phase boundaries in $Cr_2B_7O_{13}Cl$ crystals. The formulae for p_{opt} have been derived from (1) by neglecting small values of $\sin^2\varphi_{ab} \to 0$. Only the values of p_{opt} satisfying the physical sense (i.e. $0 \leqslant p_{opt} \leqslant 1$) have been considered in the table. A violation of the conditions from (2) leads to the formation of stressed phase boundaries which may take a conic shape. All the orientations $(h\,k\,l)$ have been determined in the system $(X_1X_2X_3)$ (see figure 2).

Domains T_f of the $\bar{4}2m$ phase	Domain pairs $(m;n)$ of the $mm2$ phase	Corresponding distortion matrices	Formulae for optimal volume concentrations p_{opt} in domain pairs $(m;n)$	Corresponding values of p_{opt}	sgn D'^2_{ij}		Orientations $(hkl)_{cub}$ of phase boundaries (zero-net-strain planes)
					D'^2_{12}	D'^2_{13}	
T_1	(1; 2)	$\|N^{(1)}\|, \|P^{(1)}\|$	$p_{opt} = \frac{-\epsilon_a \pm \eta_a}{\epsilon_b \cos\varphi_{ab} - \epsilon_a}$	0.391	> 0	> 0	(031) & $(03\bar{1})$
			$p_{opt} = \frac{-\epsilon_b \pm \eta_a}{\epsilon_a \cos\varphi_{ab} - \epsilon_b}$	0.609	> 0	> 0	(780) & $(7\bar{8}0)$
	(3; 4)	$\|N^{(1)}\|, \|P^{(2)}\|$	$p_{opt} = \frac{-\epsilon_a \pm \eta_a}{\epsilon_b \cos\varphi_{ab} - \epsilon_a}$	0.391	> 0	< 0	—
			$p_{opt} = \frac{-\epsilon_b \pm \eta_c}{\epsilon_a \cos\varphi_{ab} - \epsilon_b}$	0.237	< 0	> 0	—
	(5; 6)	$\|N^{(1)}\|, \|P^{(3)}\|$	$p_{opt} = \frac{-\epsilon_a \pm \eta_c}{\epsilon_b \cos\varphi_{ab} - \epsilon_a}$	0.765	< 0	> 0	—
			$p_{opt} = \frac{-\epsilon_b \pm \eta_a}{\epsilon_a \cos\varphi_{ab} - \epsilon_b}$	0.609	> 0	> 0	(340) & $(3\bar{4}0)$
T_2	(1; 2)	$\|N^{(2)}\|, \|P^{(1)}\|$	see T_1 (3; 4)	0.391	< 0	> 0	—
				0.237	> 0	< 0	—
	(3; 4)	$\|N^{(2)}\|, \|P^{(2)}\|$	see T_1 (1; 2)	0.391	> 0	> 0	(013) & $(01\bar{3})$
				0.609	> 0	> 0	(708) & $(70\bar{8})$
	(5; 6)	$\|N^{(2)}\|, \|P^{(3)}\|$	see T_1 (3; 4)	0.391	< 0	> 0	—
				0.237	> 0	< 0	—
T_3	(1; 2)	$\|N^{(3)}\|, \|P^{(1)}\|$	see T_1 (5; 6)	0.765	< 0	> 0	—
				0.609	> 0	> 0	(430) & $(4\bar{3}0)$
	(3; 4)	$\|N^{(3)}\|, \|P^{(2)}\|$	see T_1 (5; 6)	0.765	> 0	< 0	—
				0.609	> 0	> 0	(403) & $(40\bar{3})$
	(5; 6)	$\|N^{(3)}\|, \|P^{(3)}\|$	see T_1 (1; 2)	0.391	> 0	> 0	(301) & $(30\bar{1})$
				0.609	> 0	> 0	(870) & $(8\bar{7}0)$

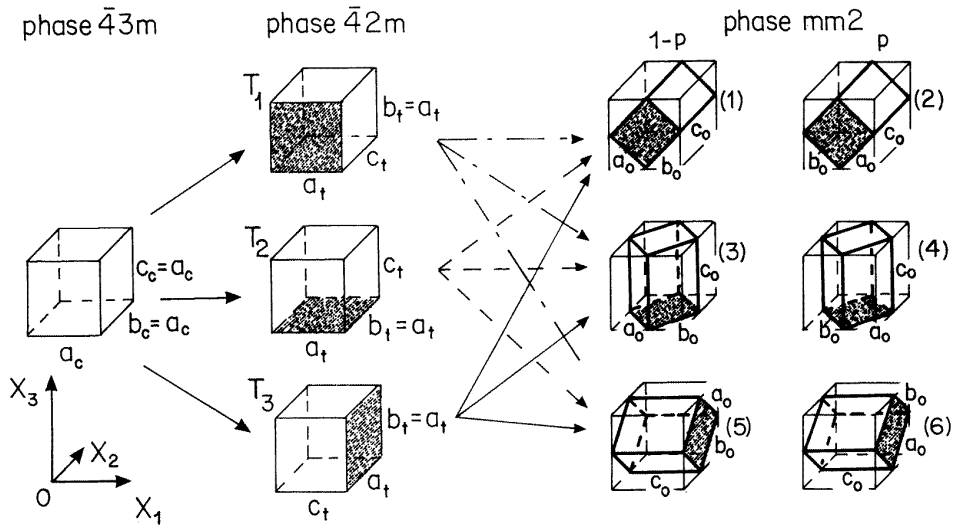

Figure 2. Possible orientations of domains which may appear at the $\bar{4}3m \rightarrow \bar{4}2m \rightarrow mm2$ phase transitions in Cr–Cl boracite crystals. a_c is the unit cell parameter in the $\bar{4}3m$ phase, a_t and c_t are the unit cell parameters in the $\bar{4}2m$ phase and a_0, b_0 and c_0 are the unit cell parameters in the $mm2$ phase. T_1, T_2 and T_3 are domains of the $\bar{4}2m$ phase. (1; 2), (3; 4) and (5; 6) are domain pairs of the $mm2$ phase characterized by volume concentrations p and $(1-p)$. The axes of the Cartesian coordinate system $(X_1X_2X_3)$ are oriented parallel to the cubic axes in the $\bar{4}3m$ phase.

account more precisely the role of the external stress and the elastic properties of crystals. A more detailed description of the features of phase coexistence at the external stress-induced phase transition supposes a marked modification of the crystallographic algorithm [9] and will be given elsewhere [19].

It has been established above that the $\bar{4}3m \rightarrow \bar{4}2m$ phase transition may take place with an active role of the internal mechanical stress. As for the elastic matching between the $\bar{4}3m$ and $mm2$ phases, there are also different possibilities for the zero-net-strain planes to exist. These possibilities may be considered analogously using the matrices $\|N^{(f)}\|$ and $\|P^{(g)}\|$ by substitutions $\eta_a \rightarrow 1$ and $\eta_c \rightarrow 1$, corresponding to the matrix $\|M\|$ (instead of $\|N^{(f)}\|$) for the unstrained $\bar{4}3m$ phase.

4. Conclusions

The formation of the $mm2$ phase, which is induced by the internal stress generated at the mechanically non-matching $\bar{4}3m$–$\bar{4}2m$ phase boundaries, has been analysed from a crystallographic point of view by taking into account the unit cell spontaneous deformation related to the first-order $\bar{4}3m$–$\bar{4}2m$ phase transition in Cr–Cl boracite. Different possibilities have been demonstrated, on the basis of determination of the zero-net-strain planes, for the transition from the tetragonal phase or the cubic phase to the orthorhombic phase in the presence of internal stress. The appearance of the $mm2$ phase satisfies the conditions for stress relief at the $\bar{4}2m$–$mm2$ and $\bar{4}3m$–$mm2$ phase boundaries. Such an unusual compromise role of the stress-induced $mm2$ phase permits us to understand the mechanism of the induced

phase transition and to interpret the three-phase coexistence at the $\bar{4}3m$–$\bar{4}2m$ transition. It may also be available for interpretation of the phase coexistence in other cases, e.g., in $PbZrO_3$ crystals, where the phase transitions $Pm\bar{3}m$–$R3m$–$Pbam$ take place within narrow temperature intervals [13], the low-temperature phase $Pbam$ may favour stress relief in the crystals [20].

Acknowledgments

The authors would like to express their thanks to Professor Hans Schmid for his constant interest in this research and for his critical review of the manuscript. This work was supported in part by the Swiss National Science Foundation (FNRS).

References

[1] Ye Z-G, Rivera J-P and Schmid H 1990 *Ferroelectrics* **106** 87
[2] Mao S-Y, Kubel F, Schmid H and Yvon K 1991 *Acta Crystallogr.* B **47** 692
[3] Ye Z-G, Rivera J-P and Schmid H 1991 *Ferroelectrics* **116** 251
[4] Ye Z-G, Rivera J-P and Schmid H 1991 *Phase Transitions* **33** 43
[5] Ye Z-G, Burkhardt E, Rivera J-P and Schmid H 1995 *Ferroelectrics* **172** 257
[6] Ye Z-G, Rivera J-P, Burkhardt E and Schmid H 1991 *Phase Transitions* **36** 281
[7] Ye Z-G, Rivera J-P, Schmid H, Hiada M and Kohn K 1994 *Ferroelectrics* **161** 99
[8] Rivera J-P 1994 *Ferroelectrics* **161** 165
[9] Metrat G 1980 *Ferroelectrics* **26** 801
[10] Topolov V Yu, Balyunis L E, Turik A V and Fesenko O E 1990 *Ferroelectrics* **110** 41
[11] Topolov V Yu 1989 *Izv. Akad. Nauk. Ser. Fiz.* **53** 1284 (Engl. Transl. *Bull. Acad. Sci. USSR Phys. Ser.* **53** 51)
[12] Topolov V Yu, Rabe H and Schmid H 1993 *Ferroelectrics* **146** 113
[13] Topolov V Yu, Turik A V, Fesenko O E and Eremkin V V 1995 *Ferroelectrics Lett. Sec.* **20** 19
[14] Aizu K 1970 *Phys. Rev.* B **2** 754
[15] Topolov V Yu and Turik A V 1990 *Izv. Vuzov. Fiz.* No 3, 68 (Engl. Transl. *Sov. Phys. J.* **33** 260)
[16] Mao S-Y, Kubel F, Schmid H and Yvon K 1992 *Ferroelectrics* **132** 239
[17] Topolov V Yu, Gagarina E S and Tsikhotskii E S 1992 *Sov. Phys.–Crystallogr.* **37** 227
[18] *Landolt–Börnstein New Series* 1990 Group III, vol 28, sub vol a, ed T Mitsui and E Nakamura (Berlin: Springer)
[19] Topolov V Yu and Ye Z-G *Ferroelectrics Lett. Sec.* at press
[20] Topolov V Yu, Balyunis L E, Turik A V, Eremkin V V and Ibrahima Sary Bah 1992 *Kristallografiya* **37** 433 (Engl. Transl. *Sov. Phys.–Crystallogr.* **37** 223)